catalysts

MDPI

Article

Cobalt-/pH-Modified V_2O_5-MoO_3/TiO_2 Catalyst with Enhanced Activity for the Low-Temperature Selective Catalytic Reduction Process

Ruonan Wang, Yanli Zhang, Xing Fan and Jian Li *

Key Laboratory of Beijing on Regional Air Pollution Control, Beijing University of Technology, Beijing 100124, China
* Correspondence: ljian@bjut.edu.cn; Tel.: +86-010-6739-2080

Abstract: Currently, the elimination of gaseous pollutants—particularly nitrogen oxides—has emerged as a significant concern. Among various deNO_x technologies, selective catalytic reduction (SCR) has gained prominence as the primary approach for NO_x abatement, owing to its superior performance. In this study, novel low-temperature SCR catalysts were developed by regulating the pH value and doping cobalt based on a V_2O_5-MoO_3/TiO_2 (VMT) catalyst. The results show an increased SCR performance with 82.8% and 91.1% for catalysts after pH (=10) modification (VMT-10) and (1 wt%) Co/pH (=10) modification (1CoVMT-10), respectively. H_2-TPR, NH_3-TPD, XPS and DRIFTS confirmed that the pH regulation transformed polymerization V species into isolated V^{5+}=O, thus leading to an increase in the number of acid sites, which enhanced the NH_3 and NO_2 adsorption capacity. Furthermore, the DRIFTS study indicated that the NH_3-SCR reaction over 1CoVMT-10 followed the E–R and L–H mechanism.

Keywords: selective catalyst reduction; cobalt doping; pH regulation; modified catalyst; low temperature

Citation: Wang, R.; Zhang, Y.; Fan, X.; Li, J. Cobalt-/pH-Modified V_2O_5-MoO_3/TiO_2 Catalyst with Enhanced Activity for the Low-Temperature Selective Catalytic Reduction Process. *Catalysts* **2023**, *13*, 844. https://doi.org/10.3390/catal13050844

Academic Editors: Haidi Xu and Honggen Peng

Received: 8 March 2023
Revised: 20 April 2023
Accepted: 4 May 2023
Published: 6 May 2023

1. Introduction

As a main contaminant in steel and coal-fired industries, photochemical smog, acid rain, and the damage to human health caused by NO_x urgently requires solutions. Selective catalytic reduction (SCR) is the main method for NO_x removal due to its high performance among various deNO_x technologies. V_2O_5-MoO_3(WO_3)/TiO_2 catalysts have been widely commercialized in industrial NO_x removal, operated at temperatures ranging from 280 °C to 400 °C. V_2O_5-MoO_3(WO_3)/TiO_2 (VM(W)T) is one of the most widely used catalysts for the NH_3-SCR process at present. The market for high-temperature catalysts has matured due to the installation of denitration devices in the front of dust and sulfur removal equipment [1]. However, the existing high amount of dust delivered a negative effect on catalysts; high-concentration dust contains a large number of harmful elements, such as Na, K, Ca, and As, which will poison the catalyst. Therefore, novel SCR units are commonly installed downstream of the airflow (approximately 180–200 °C) to the dust collector, necessitating the use of low-temperature SCR catalysts capable of performing denitrification. Moreover, anatase TiO_2, which plays an important carrier role in VM(W)T catalysts, is susceptible to sintering at high temperatures, and the resultant crystal phase conversion can lead to catalytic activity reduction [2,3]. Hence, developing highly efficient catalysts for low-temperature NO_x conversion seems imperative.

The properties of V_2O_5-MoO_3(WO_3)/TiO_2 catalysts have been extensively investigated. Denitrification activity can be effectively enhanced by including WO_3 and MoO_3 (especially at amounts of 10% and 6%, respectively) in the composite [3–5]. Modifying SCR catalysts with other additives, such as transition metals, is another way to develop better catalytic behavior [6–9].

Cobalt oxide (CoO_x) has proven to be one of the most efficient metal oxide catalysts for increasing the removal of N_2O, CH_4, and NO due to its excellent reduction ability and abundant oxygen vacancy [9,10]. For example, the effect of Co/ZSM proved that the ammonia species adsorbed on the Brønsted acid site and that $–NH_2$ may take part in the medium/low-temperature region in the NH_3-SCR process [11]. A catalyst consisting of K and Co_3O_4 could promote the availability of Co^{2+} by effectively regenerating the Co^{3+} oxidized by N_2O [12]. For Co–Ce binary metal oxide catalysts, the redox pair of Ce^{3+}/Ce^{4+} in CeO_2 facilitates the storage and release of lattice oxygen species, re-oxidizing Co^{2+} to Co^{3+} [13]. In addition, the participation of Co in the catalyst can simultaneously increase the activity of both O_α and O_β and L–H (Langmuir–Hinshelwood mechanism) was also proposed according to the source of active oxygen species [14].

Apart from modifying catalysts with various elements, pH regulation could be regarded as another effective way to improve SCR activity. A one-step ion exchange method was used to increase the amount of Cu^{2+} by changing the pH of the precursor mixture with HNO_3, in which the H^+ concentration has a significant influence on the Cu loading and distribution [15]. A series of Mn-doped perovskite La–Mn oxides were prepared during the synthesis with ammonia, while Mn^{4+} content was dominant when regulating the pH to 1.4, which displayed excellent NH_3-SCR activity [16]. In another study, ammonium hydroxide was successfully used to reduce aggregated polymerization in V_2O_5/TiO_2 catalysts, and the as-obtained isolated vanadium species mainly worked on the adsorption and oxidation of NH_3, resulting in higher NO_x conversion [17].

In previous tests, a VMT catalyst prepared in our laboratory could maintain a denitrification efficiency of over 85% under factory conditions, but this is not enough for low-temperature SCR catalysts with better efficiency and stability. In this work, modified V_2O_5-MoO_3/TiO_2 (VMT) catalysts generated by pH (=10) regulation (VMT-10) and recombined (1 wt%) cobalt doping (1CoVMT-10) were investigated. The purpose of the present work is to clarify the impact of Co/pH affected by the physicochemical properties and catalytic performance of VMT catalysts; the structures of the catalysts were characterized by XRD, BET, SEM, H_2-TPR, NH_3-TPD, and in situ DRIFTS.

2. Results and Discussion

2.1. NH_3-SCR Activity

The parameters that varied during the experiments were the amount of Co doping and the pH regulation value. The samples were herein denoted as xCoVMT-y, where x is the mass fraction of Co (x = 1, 3, 5), while y is the pH (y = 9, 9.5, 10, 10.5, 11).

The addition of Co was initiated during impregnation. Based on Figure 1a–c, the denitration efficiency of the catalysts at different pH values changed as a function of Co addition (1, 3, and 5 wt%). Figure 1a shows that the NO_x conversion rate was 71.4% at 160 °C for unmodified VMT. For the 1CoVMT sample series, at the investigated pH 9–11 interval, the best catalyst (1CoVMT-10) developed to 91.1% denitrification efficiency was observed at pH 10, which was 19.7% higher than that for the VMT reference. By increasing the amount of Co (Figure 1b,c), the most efficient activity decreased to 89.3% (3CoVMT-10) and 85.8% (5CoVMT-10).

The NO_x removal efficiency decreased with the increased Co addition after pH adjustment (Figure 1d), suggesting that excessive Co has an inhibitory effect on the catalyst. Probably, an increase in active components unavoidably resulted in increasing particle sizes and the formation of polymeric constituents or large grains on the surface. This further reduced the capacity of the catalyst to activate molecular oxygen and remove lattice oxygen [18].

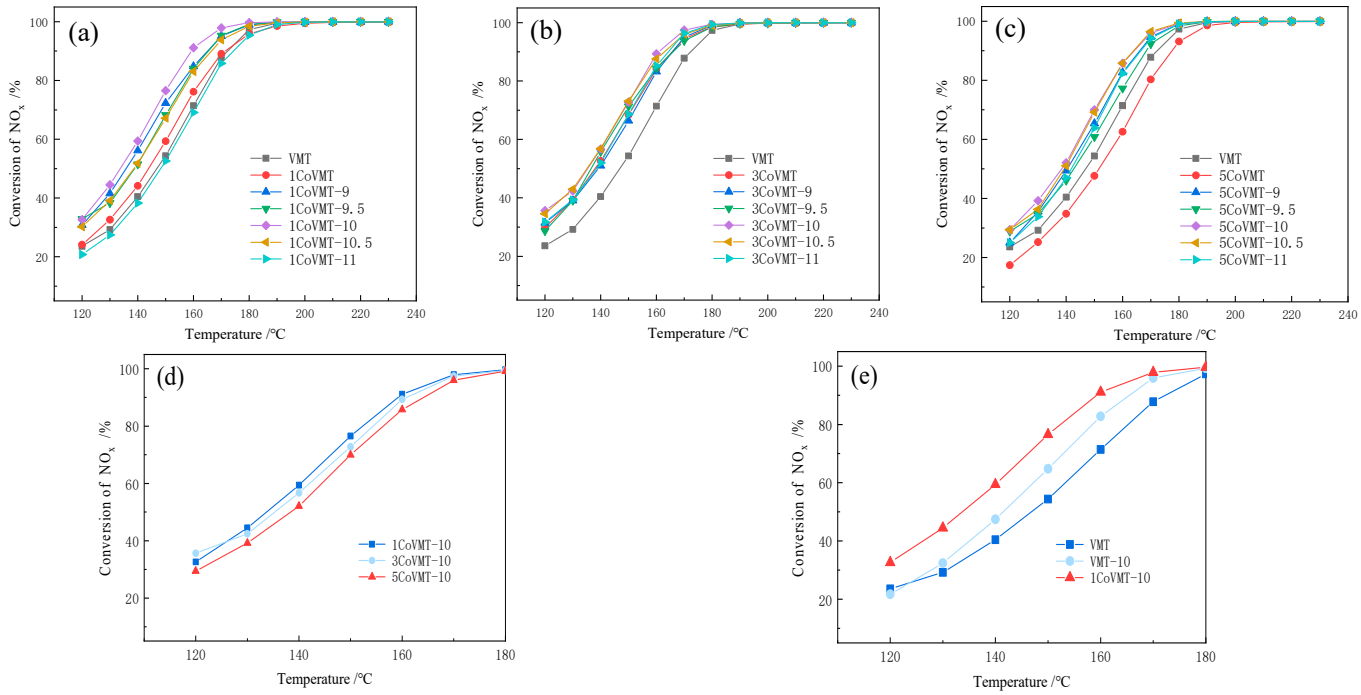

Figure 1. NH_3-SCR activity: (**a**) 1CoVMT series; (**b**) 3CoVMT series; (**c**) 5CoVMT series; (**d**) 1Co/3Co/5CoVMT-10; (**e**) VMT/VMT-10/1CoVMT-10.

For further investigation, the NO_x conversion curves of VMT, VMT-10, and 1CoVMT-10 are compared in Figure 1e. The catalytic efficiency could be improved both by increasing the pH value and the amount of Co. Two parameters synergistically promoted the NO_x conversion efficiency of the catalysts. Table S1 lists the NO removal efficiency under laboratory conditions of Co-doped or pH-regulated catalysts. Compared to previous studies, it can be seen that current research has a wider temperature range under low-temperature testing conditions and has an advantage in denitrification efficiency at higher NO_x concentration.

2.2. Textural Properties

The catalysts prepared by adjusting the pH and adding different amounts of Co were compared with VMT. The results were evaluated using the BET and BJH methods, as shown in Table 1, and the calculated value of C = 71 falls within the applicable range for oxides (Figure S1).

Table 1. Pore structure parameters.

Sample	pH Value	Specific Surface Area $A/(m^2 \cdot g^{-1})$	Pore Volume $v/(cm^3 \cdot g^{-1})$	Average Pore Diameter d/(nm)
VMT	2.5	72	0.31	17.1
VMT-10	10	78	0.37	18.8
1CoVMT-10	10	75	0.37	19.9

Adjusting the pH value resulted in larger specific surface areas, pore volumes, and pore diameters. However, simultaneous Co/pH modification reduced the specific surface area, which might be ascribed to the blockage of partial pores caused by cobalt impregnation.

Figure 2a–c show the adsorption isotherms and pore size distributions of VMT, VMT-10, and 1CoVMT-10, wherein all samples could be characterized by a type IV isotherm [19]. Mesopores were also present according to the hysteresis loops. The pore structure provided numerous active sites for gas molecules. For 1CoVMT-10, the enlarged hysteresis loop

indicates that gas adsorption and diffusion are facilitated in this sample, thus increasing the catalytic reaction (Figure 2c). In Figure 2d, the pore distributions of the three catalysts are compared. As a result of pH modification, the number of micropores increased (both VMT-10 and 1CoVMT-10), whereas the addition of Co had little effect on the pore size distribution. It can be speculated that the influence of the Co content on the pore structure damage is limited. Variations in pore structure caused by adjusting the pH were likely to be one of the most important reasons for the improved denitrification efficiency.

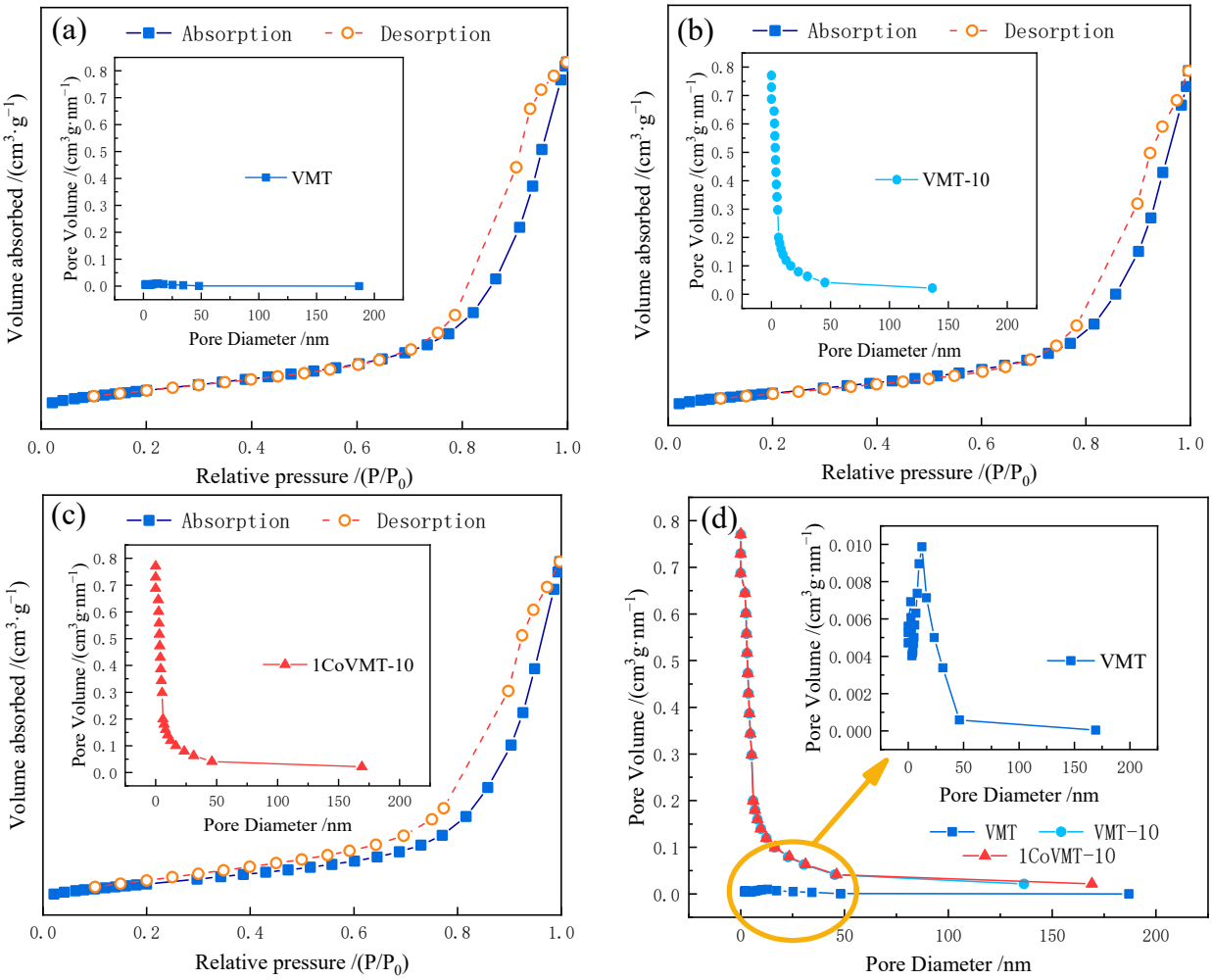

Figure 2. N_2 adsorption–desorption isotherms and pore size distribution: (**a**) VMT; (**b**) VMT-10; (**c**) 1CoVMT-10; (**d**) Sample comparison of pore size distribution.

Based on the SEM images of VMT (Figure 3a), the rough surface with large particles developed a relatively flat appearance with small pores after pH regulation (VMT-10; Figure 3b). For the visibly deeper cracks and pores detected on the surface of VMT, the particles in VMT-10 are more compact, and the cracks become narrower. This might be due to the transformation of polymeric V–O–V bonds into isolated V=O bands [20]. Then, after Co/pH modification, the surface particles became even finer, indicating that Co doping also had an isolated dispersion influence on the catalyst (Figure 3c). The labeled area consists of small particles and is distributed more uniformly on the surface. As the 1CoVMT-10 catalyst had the best efficiency, it is suggested that partially isolated species might play an advantageous role in terms of catalyst activation [6].

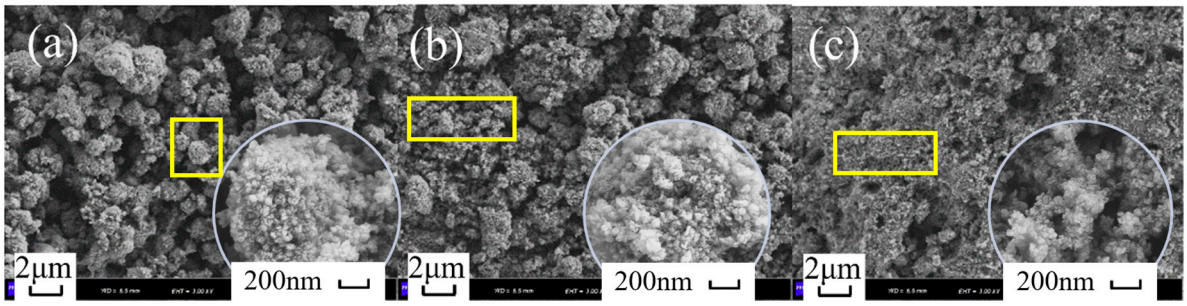

Figure 3. SEM images of catalyst surface: (**a**) VMT; (**b**) VMT-10; (**c**) 1CoVMT-10.

2.3. XRD Measurement

The diffraction peaks at 25.3°, 37.8°, 48°, 54°, 55°, 62.8°, 69°, 70.3°, and 75° were attributed to anatase TiO_2 (Figure 4). No rutile crystal phase and active components (CoO_x, VO_x, MoO_x) were observed during XRD analysis, suggesting that they were well-dispersed on the support structure, or the amount of rutile crystal phase and active components were too low to be detected.

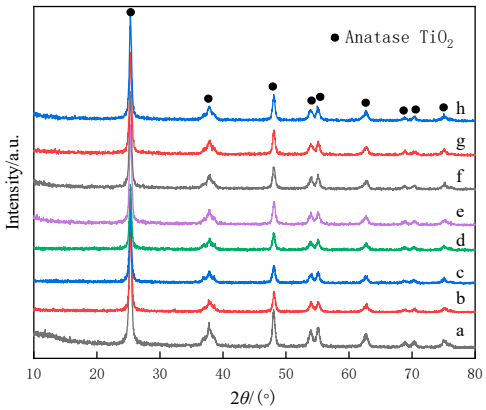

Figure 4. XRD patterns of the catalyst samples: (a) VMT; (b) 1CoVMT; (c) 3CoVMT; (d) 5CoVMT; (e) VMT-10; (f) 1CoVMT-10; (g) 3CoVMT-10; (h) 5CoVMT-10.

2.4. H_2-TPR Experiments

H_2-TPR measurements were carried out for the samples. As shown in Figure 5, 3 T_{max} types could be observed: isolated monomeric species (≤497–507 °C), polymeric species (537 °C), and bulk amorphous V_2O_5 (579 °C) [20]. The difference observed for VMT and VMT-10 at 413 °C and 429 °C, respectively, in Figure 5a, indicated that isolated monomeric species could be caused by ammonium hydroxide. For polymeric and bulk amorphous species, due to overlapping characteristic peaks, we conducted peak separation analysis for the two peaks at 537 °C and 579 °C, as seen in Figure S2, and filled the peak area of vanadyl species from the fitting data present in Table S2. The results showed that the monomeric species of the VMT catalyst accounted for approximately 60.7%, and after the addition of NH_4OH, the proportion of monomeric species in the catalyst increased to 78.6%. Furthermore, the monomeric species of the 1CoVMT-10 catalyst reached the maximum proportion to 79.4%, and its bulk amorphous species decreased to the lowest value among the three catalysts, indicating that the modification indeed increased the quantity of the monomeric species on the catalyst surface. According to the research of *S. Besselmann*, polymeric and crystal vanadiums on V/Ti catalysts can be selectively removed after washing with aqueous ammonia, resulting in monomeric species [17]. It is generally believed that monomeric V species activate catalysts better than polymerized V_2O_5 [21]. The reaction of H_2 with V^{5+} eventually generates V^{3+} [22]. The peak at 700 °C is

characteristic of the transformation of V_2O_5 to V_6O_{13} [21], while others believe that it could also be due to the decomposition of bulk V_2O_5 [20].

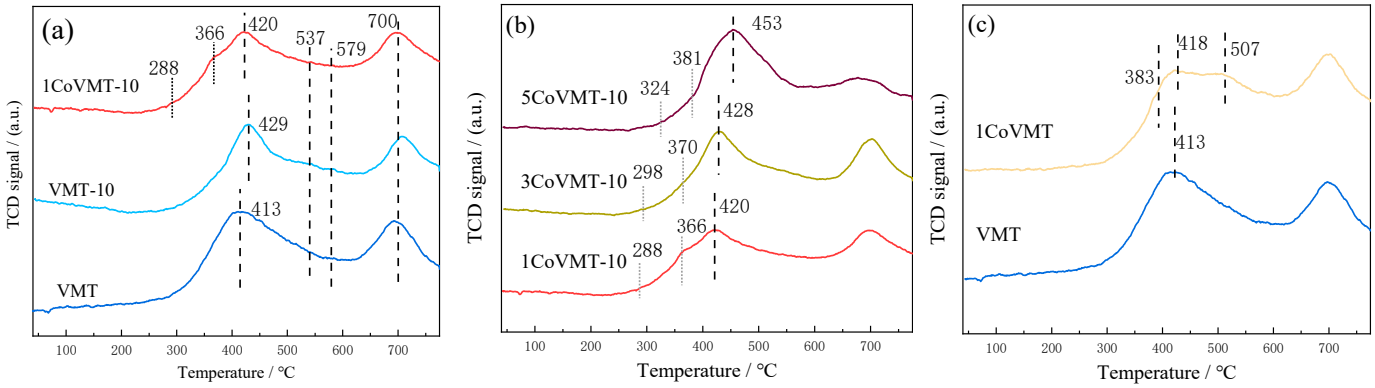

Figure 5. H_2-TPR profiles of the catalyst samples: (**a**) VMT/VMT-10/1CoVMT-10; (**b**) 1Co/3Co/5CoVMT-10; (**c**) VMT/1CoVMT.

Vanadium can form many different compounds depending on the chemical properties of the solution. For example, VO_4^{3-} and $VO_3(OH)^{2-}$ ions mainly exist in strong alkaline media [6]. For VMT-10, the decreased height in the 480–560 °C range indicates the lack of polymerization (Figure 5a). Furthermore, the generated isolated V=O on Brønsted acid on V/Ti catalysts has proven to play a significant role in SCR [20,21].

At 288 °C and 366 °C (Figure 5a), cobalt provided new reduction sites, while the former belongs to the transformation of Co^{3+} to Co^{2+}, and the latter belongs to the transformation of Co^{2+} to metallic Co. [12]. For the Co reduction peaks, the peak at 366 °C for Co^{2+} is more pronounced for 1CoVMT-10, while the peak of Co^{3+} is relatively weak. With an increase in Co%, the characteristic peaks of both Co^{3+} and Co^{2+} shifted to higher temperatures, gradually approaching the characteristic peak of vanadyl monomeric species until partially overlapping, as shown in Figure 5b. When Co% was added excessively, vanadyl species reduction peaks gradually shifted from 420 °C to 428 °C and 453 °C for 1Co, 3Co, and 5Co, respectively. The peak shift here is probably due to the transformation of vanadyl species from monomeric species to polymeric species. The shift toward higher temperatures caused by excess Co addition is detrimental to the conversion of NO to NO_2 [23], as low-temperature reducibility was one of the key factors affecting catalytic activity [24].

During H_2-TPR measurements, the effects of Co doping were also investigated in Figure 5c. After 1 wt% cobalt doping, a peak with a broad shoulder was observed at 507 °C, which indicates that the presence of isolated V species and a few polymeric V species consumes large amounts of hydrogen. It was found that appropriate polymerization can improve reaction activity [6], and this heterogeneous structure is formed to produce with a unique effect to catalytic performance improvement.

2.5. XPS Measurement

The XPS corresponding spectra of Co $2p_{3/2}$, O 1s, and V $2p_{3/2}$ are illustrated in Figure 6, and the surface binding energies and ratio of the valence state are summarized in Table 2. For 1CoVMT-10, Co^{2+} (782.2 eV) shows a dominant amount compared to Co^{3+} (779.9 eV) [25], as seen in Figure 6a. The ratio of Co^{2+}/Co^{3+} is large, which is 5.00 to 1CoVMT-10, indicating that Co^{2+} has high activity in the SCR reaction. As the percentage of Co in the catalyst increases, a decrease in the proportion of Co^{2+} and a concomitant increase in the proportion of Co^{3+} was observed.

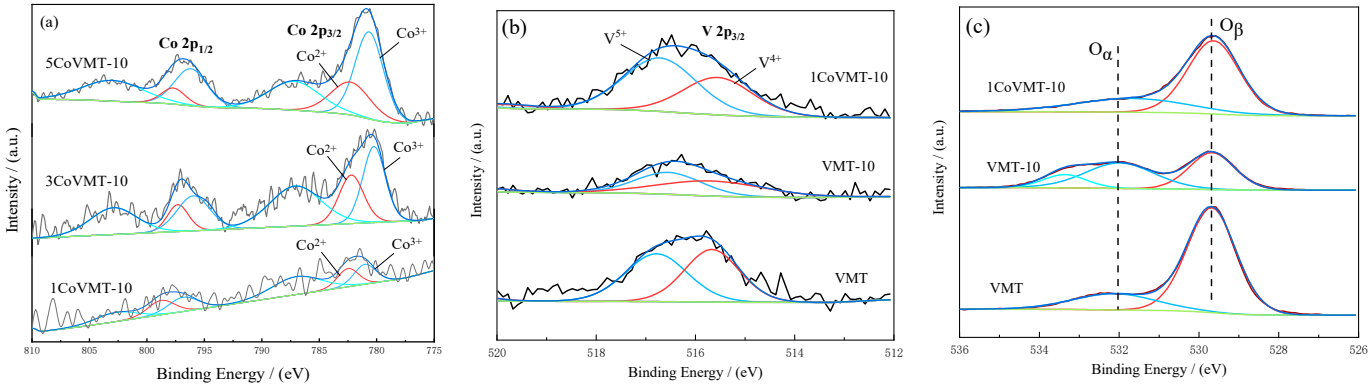

Figure 6. XPS profiles of catalyst samples: (**a**) Co; (**b**) V; (**c**) O.

Table 2. Surface binding energies and ratio of valence state.

Sample	Binding Energy (eV)			Ratio of Valence State		
	Co 2p Co^{2+} Co^{3+}	O_α O_β	V 2p V^{4+} V^{5+}	V^{5+}/V^{4+}	$O_\alpha/(O_\beta + O_\alpha)$	Co^{2+}/Co^{3+}
VMT	—	532.5 529.6	515.7 516.8	1.02	14.11	—
VMT-10	—	532.0 529.8	515.7 516.6	1.12	58.34	—
1CoVMT-10	782.2 779.9	532.3 529.5	515.6 516.7	1.49	16.30	5.00

From Figure 6b and Table 2, the V $2p_{3/2}$ peaks are concentrated at 514–518 eV, which are attributed to V^{5+} and V^{4+} characteristic peaks. V^{4+} ions were abundant in VMT, but the growing ratio of V^{5+}/V^{4+} brought about pH regulation and Co doping in VMT-10 and 1CoVMT-10 indicates that V^{5+} has higher activity in the SCR reaction. However, the amount of V shows a certain decrease in VMT-10. When Co was added, the total amount of V was readded. The presence of Co^{2+} and V^{5+} enables the $Co^{2+} + V^{5+} \rightarrow Co^{3+} + V^{4+}$ reaction. NH_4^+ adsorbed on V=O reacts with Co^{3+} to form NH_3^+ by dehydrogenation, and the obtained NH_3^+ combined NO to produce H^3N^+NO, which finally decomposed to H_2O and N_2. Then, the increasing synergized Co^{2+} could be oxidized by V^{5+}, while V^{4+} was oxidized by O_2, respectively.

Modifying the pH affected the distribution of lattice oxygen and adsorbed oxygen significantly. In Figure 6c, the O 1s spectrum is commonly divided into two components: oxygen species at 529–531 eV (lattice oxygen species; O_β), and 531–534 eV (adsorbed oxygen species; O_α). From Table 2, affected by the ammonia solution, the ratio of $O_\alpha/(O_\beta + O_\alpha)$ in VMT-10 greatly increased from 14.11% to 58.34%.

Considering the high mobility of O_α, the larger ratio of $O_\alpha/(O_\alpha + O_\beta)$ is beneficial for yielding improved catalytic activity [26]. VMT-10 exhibited the highest proportion of adsorbed oxygen ($O_\alpha/(O_\beta + O_\alpha)$) at 58.34%. Massive surface adsorbed oxygen was favorable to the recirculation of reactive oxygen species, which was also an advantage for the improvement of catalyst activity [24].

Co doping restored the amount of O_β in 1CoVMT-10 (Figure 6c). Since oxygen vacancies were generated to balance the decreasing charge of Co^{3+}, the ratio of Co^{2+}/Co^{3+} for 5.00 was considered to be indicative of the creation of oxygen vacancies on the surface. It is possible that the increase in crystal oxygen is caused by the addition of Co oxides, which leads to the formation of surface oxygen vacancies, as Co^{3+} is converted to Co^{2+} [27]. The generation of V^{5+}, together with the observation of Co^{2+} species, was demonstrative of the synergetic effect between vanadium and cobalt via charge transfer ($V^{5+} + Co^{2+} \leftrightarrow V^{4+} + Co^{3+}$), which further confirmed the earlier deduction from H_2-TPR.

In addition, studies have shown that both O_β and O_α could promote the participation of active substances in the process of oxidizing NO to NO_2, theoretically making the rapid SCR cycling reaction ($2NH_3 + NO + NO_2 \rightarrow 2N_2 + 3H_2O$) easier to occur [27,28], related to

higher SCR activity. O_β and O_α play different roles throughout the entire SCR process. For the VMT-10 catalyst, the advantages introduced by O_α dominated and chemisorbed oxygen had a significant effect on the deep oxidation reactions of the reducing substances [29]. For the 1CoVMT-10 catalyst with the added Co element, O_β is more advantageous. Maintaining the continuity of surface oxygen vacancies in the catalyst is one of the main factors affecting the catalyst activity [30].

2.6. NH_3-TPD Measurement

For the NH_3-SCR method, the basic reaction gas of NH_3 first adsorbs on the acid sites and then participates in SCR [31].

Acid sites can be classified according to their thermal stability: weakly (physically) adsorbed NH_3 (100–250 °C), NH_3 adsorbed on Lewis acid sites (250–350 °C), and NH_3 adsorbed on Brønsted acid sites (over 350 °C) for chemisorption [32,33]. As illustrated in Figure 7a, all of the samples exhibited similar peaks at around 93 °C, which were attributed to weakly (physically) adsorbed NH_3. The adsorption peaks at around 350 °C and 435 °C were attributed to NH_3 adsorbed at the Lewis acid site, and the peak at 655 °C corresponded to the NH_3 bound at Brønsted acid sites (NH_4^+) [34].

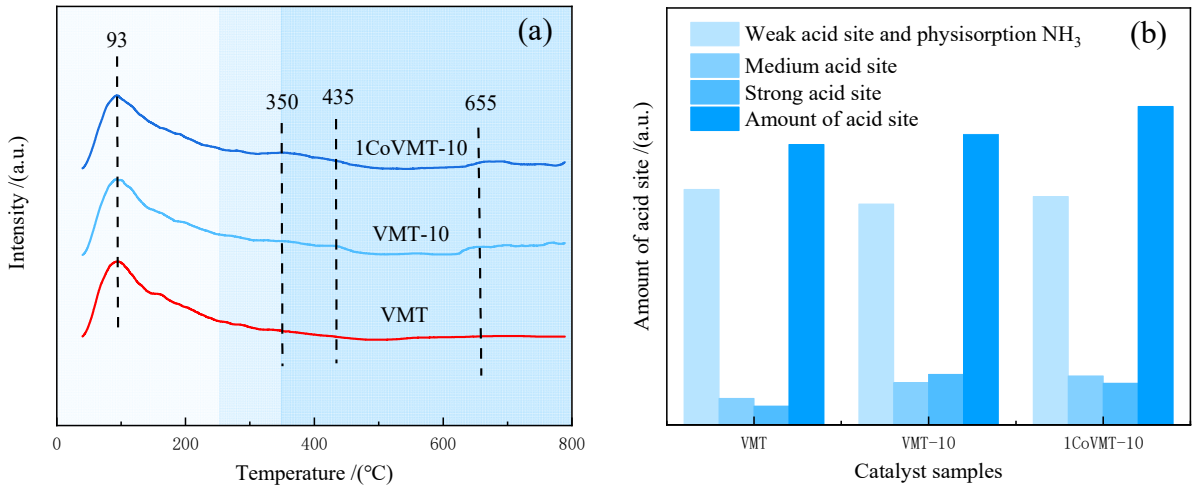

Figure 7. (**a**) TPD profiles of catalyst samples; (**b**) Distribution of various acidic sites.

In Figure 7b, a gradual increase in the content of basic sites brought about through pH regulation and Co doping also indicated the strengthened ability for NH_3 adsorbed on the catalyst surface. The increased number of strong acid sites on VMT-10 was attributed to the formation of strong isolated V=O bonds, suggesting that VMT-10 and 1CoVMT-10 possessed stronger acid sites. Compared to VMT-10, the 1CoVMT-10 catalyst had more sites at 350 °C and 435 °C, indicating that Co species improved the ability to bind NH_3 at Lewis acid sites in the medium region. Additionally, the result goes some way toward reflecting that abundant acid sites had better efficiency in terms of catalytic behavior.

2.7. In Situ Drifts Measurement

2.7.1. Adsorption of NH_3

Previous studies proved that NH_4^+ species adsorbed on the catalyst surface react with gaseous NO species during SCR [35]. As shown in Figure 8, after N_2 purging pretreatment at 300 °C, NH_3 was inlet and adsorbed on catalysts at ambient temperature. When the temperature gradually increased from 100 to 300 °C at a rate of 4 °C/min, infrared bands were recorded at 100 °C, 150 °C, 200 °C, 250 °C, and 300 °C, respectively.

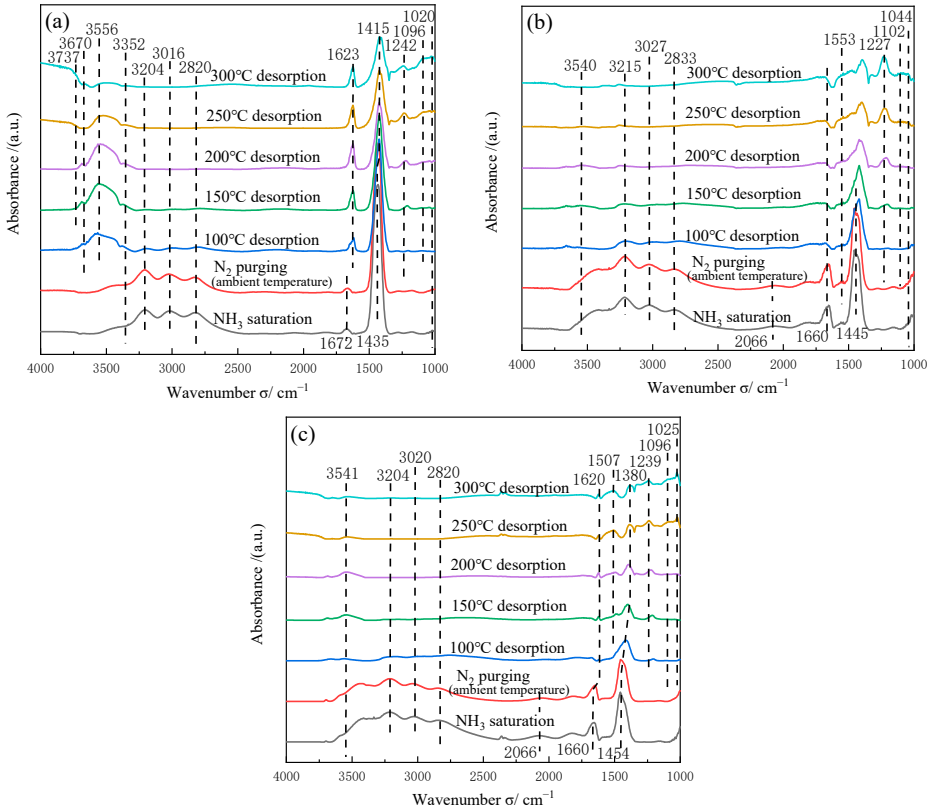

Figure 8. In situ DRIFTS patterns of catalysts exposed to 0.07 vol% NH_3 and desorption under N_2: (**a**) VMT; (**b**) VMT-10; (**c**) 1CoVMT-10.

The bands at 1435, 1445, 1672, and 1660 cm^{-1} were ascribed to the bending and symmetric bending vibrations of NH_4^+ at Brønsted acid sites [36], or the bending vibrations of N–H bonds at Brønsted acid sites originating from the chemisorption of NH_3 on the V–OH groups of the catalyst [21]. In addition, the gradually decreased peak intensities of 1445, 1454, and 1660 cm^{-1} in VMT-10 and 1CoVMT-10 indicated that the modification due to pH regulation and cobalt doping both reduced the formation of polymeric HO–V–OH bonds.

The infrared absorption bands at 1242 cm^{-1} (Figure 8a), 1227 cm^{-1} (Figure 8b), and 1239 cm^{-1} (Figure 8c) were similar to those at 1623 cm^{-1} (Figure 8a) and 1620 cm^{-1} (Figure 8c). All of them can be attributed to the asymmetric bending vibrations of the N–H bonds during the N–H chemisorption at the Brønsted acidic sites [21,37], which appeared at 150 °C and could be detected at high temperatures. The band at 3352 cm^{-1} can be ascribed to asymmetric N–H stretching vibrations at the Lewis acidic sites (Figure 8a) [37–39]. The absorption bands at 3556, 3670, and 3737 cm^{-1} were attributed to the O–H tensile vibrations caused by the interaction between surface hydroxyl groups and NH_3 [39,40]. From Figure 8a–c, the bands observed at 2820, 2833, 3016, 3020, 3027, 3204, and 3215 cm^{-1} can be attributed to NH_4^+ species [41]; meanwhile, these species could be easily desorbed at 150 °C on the catalyst surface, which was in accordance with the results of NH_3-TPD.

The bands observed at 1415 cm^{-1} and 1445 cm^{-1} on VMT can be attributed to the adsorption capacity of V_2O_5 on the catalyst surface were also related to the asymmetric bending vibrations of NH_4^+ chemisorbed on the Brønsted acid sites [26]. It is evident that among the three catalysts, 1CoVMT-10 exhibited a faster disappearance of NH_4^+ groups at these sites, indicating that the NH_4^+ groups on the surface of 1CoVMT-10 are more active. The absorption bands at 1020 and 1096 cm^{-1} (Figure 8a), 1044 and 1102 cm^{-1} (Figure 8b), and 1025 and 1096 cm^{-1} (Figure 8c) were attributed to δ_S(NH) symmetric bending vibrations at the Brønsted acidic sites. After pH regulation, the intensity of the bands on VMT-10 decreased, indicating that the transformation of $–NH_2$ into –NH was

inhibited under alkaline conditions. In conclusion, Co/pH modification improved the reductive properties of the catalysts by restricting the growth of –NH groups.

The bands at 1553, 2066 (Figure 8b), 1507, and 2066 cm^{-1} (Figure 8c) can be ascribed to N–H bonds chemisorbed on V=O Lewis acidic sites, and the lattice oxygen on V=O can react with adsorbed NH_3 [21]—these benefited from Co/pH modification. It was only VMT on which any obvious infrared absorption band could not be observed in these regions due to an insufficient number of V=O sites.

2.7.2. Reaction of NH_3 with $NO+O_2$

The reaction of catalysts with NH_3 and NO during SCR was also simulated by in situ DRIFTS. Following surface NH_3 saturation and purging with N_2, a 0.07 vol% NO and 5 vol% O_2 mixture was introduced into the reaction chamber. The spectra were recorded at different temperatures, as in Figure 9.

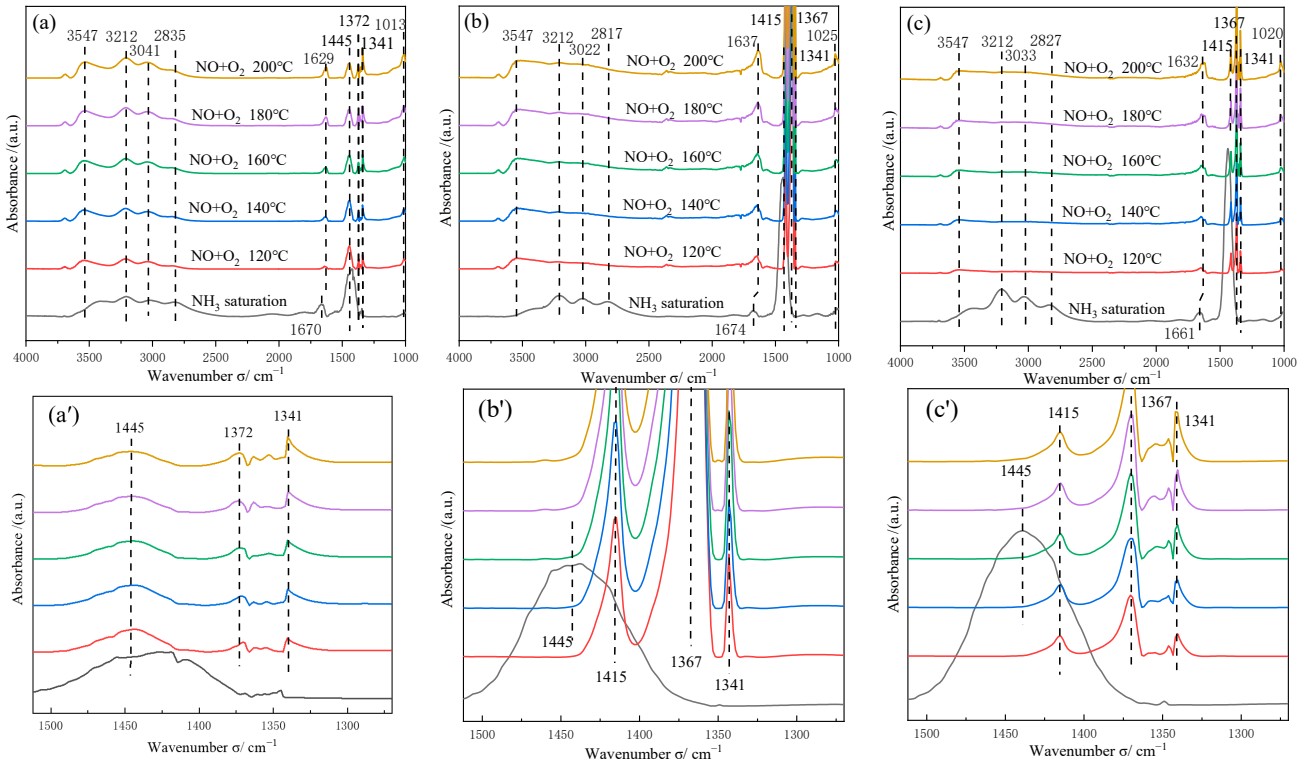

Figure 9. In situ DRIFTS patterns of catalysts exposed to 0.07 vol% NH_3 and 0.07 vol% NO + 5 vol% O_2: (**a**) VMT; (**b**) VMT-10; (**c**) 1CoVMT-10. For 1250–1500 cm^{-1}: (**a′**) VMT; (**b′**) VMT-10; (**c′**) 1CoVMT-10.

The bands at 1670, 2835, 3041 cm^{-1} (Figure 9a), 1674, 2817, 3022 cm^{-1} (Figure 9b), and 1661, 2827, 3033, 3212 cm^{-1} (Figure 9c) were attributed to the presence of NH_4^+. When reaching 120 °C, the bands from VMT-10 and 1CoVMT-10 disappeared rapidly after $NO+O_2$ exposure. This could be due to their well-developed desorption capacity to NH_3 [41]. NH_4^+ groups on the surface of VMT did not sufficiently react with $NO+O_2$ in air, as their characteristic band could still be observed at 200 °C.

Adding $NO+O_2$, NH_4^+, and NH_3 groups on the surface can generate active intermediates that react with NO_2 during SCR [37]. Characteristic bands of NO_2 were observed at 1629 (Figure 9a), 1637 (Figure 9b), and 1632 cm^{-1} (Figure 9c). It was deduced that pH regulation increased the number of Lewis acidic sites on the catalyst surface and improved its adsorption capacity for NO_2 [37,42].

We have zoomed in on the 1250–1500 cm^{-1} range of the infrared spectrum in Figure 9a′–c′. The asymmetric bending vibrations of NH_4^+ chemisorbed on Brønsted acid can be ob-

served at 1445 cm^{-1} and 1415 cm^{-1} in Figure S2 [6,26,43]. The 1341 cm^{-1} band was attributed to NO_x species, while the 1372 cm^{-1} and 1367 cm^{-1} bands corresponded to nitrate species [37,44].

The peak at 3547 cm^{-1} was attributed to the vibration of O–H in H_2O. As the temperature increased, physically adsorbed water gave rise to strong infrared bands at approximately 3550 cm^{-1} [39,45]. The VMT and VMT-10 exhibit a more prominent peak at this location, whereas the 1CoVMT-10 shows a weak and broad peak, suggesting that the adsorption of surface H_2O was suppressed at this location.

For VMT, the absorption bands at 1013 and 1629 cm^{-1} can be attributed to the NO_x species (Figure 9a); the one at 1013 cm^{-1} corresponds to the N_2O_2 group υ_{as}, while the one at 1629 cm^{-1} can be ascribed either to nitrite (NO_2^-) or nitrate (NO_3^-) [44,46,47]. The intensity of all these bands increased slightly with increasing temperature.

VMT-10 possessed the highest NO_2 band (1637 cm^{-1}) intensity (Figure 9b), indicating the formation of a strong bond between NO_2 and the Lewis acidic site during adsorption. However, too strong of adsorption inhibited the conversion of NO_x. As shown in Figure 9c, the band at 1632 cm^{-1} for 1CoVMT-10 reduced significantly compared to that for VMT-10. This proves that Co addition could compensate for the disadvantage caused by the strong adsorption [10].

2.7.3. Reaction of NH_3 and $NO+O_2$ on 1CoVMT-10

During the SCR process, the mixed atmosphere of NH_3, NO, and O_2 exposed upon Lewis and Brønsted acidic sites could be provided by V_2O_5. As shown in Figure 10, a higher adsorption strength was provided by NH_3 than for NO, indicating that the dominant reaction in SCR occurred via the E–R (Eley–Rideal) reaction mechanism [48,49].

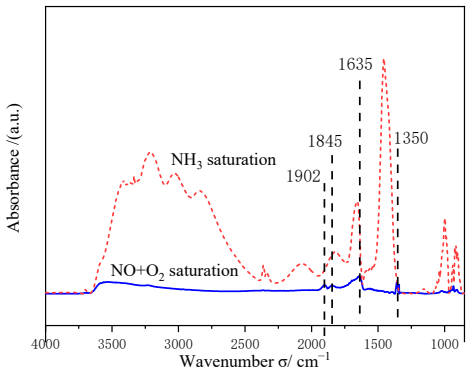

Figure 10. Comparison between the in situ DRIFTS patterns of 0.07 vol% NH_3 and 0.07 vol% NO + 5 vol% O_2 adsorbed on 1CoVMT-10.

Studies have shown that a limited amount of NO can be adsorbed on V/Ti catalysts [50,51]. Whereas, in Figure 10, the adsorption bands of NO (1902, 1845 cm^{-1}), NO_2 (1635 cm^{-1}), and $-NO_2$ (1350 cm^{-1}) could still be observed. Based on the contents mentioned above, the reaction of oxidized intermediates of NO_2 and adsorbed NH_3 on the surface of VMT-10 and 1CoVMT-10 promoted SCR, proving that this process might also follow the L–H (Langmuir–Hinshelwood) mechanism [39].

In this way, NH_3 was adsorbed on the SCR catalysts and was activated through H abstraction to form NH_2, which then reacted with the gas phase NO to form a nitroamide (NH_2NO) species. The nitrous acid was produced through a reoxidation reaction. The nitrous acid reacted with ammonia and then produced ammonium nitrite. Both ammonium nitrite and nitrosamine were unstable and would decompose into N_2 and H_2O.

The Eley–Rideal mechanism (reactions between the coordinated NH_3 and gaseous NO over the Lewis acid sites):

$$NH_3(g) + O(a) \rightarrow NH_2(a) + OH(a) \quad (1)$$

$$NO(g) + NH_2(a) \rightarrow NH_2NO(a) \quad (2)$$

$$NH_2NO(a) \rightarrow N_2(g) + H_2O \quad (3)$$

The SCR of NO with NH_3 on the V_2O_5/TiO_2 catalyst proceeds through the oxidation of NO to NO_2. NH_3 is adsorbed in the form of coordinated NH_3, NH_4^+, and $–NH_2$. V_2O_5 promotes the formation of $–NH_2$, which is the main intermediate of the SCR reaction.

Catalysts in the SCR reaction follow the Langmuir–Hinshelwood mechanism (reactions between the absorbed NO_2 and coordinated NH_3):

$$2NO + O_2(g) \rightarrow 2NO_2(a) \quad (4)$$

$$NH_3(g) \rightarrow NH_3(a) \quad (5)$$

$$NO_2(a) + 2NH_3(a) \rightarrow NO_2(NH_3)_2 \quad (6)$$

$$NO(a) + NO_2(NH_3)_2 \rightarrow 2N_2 + H_2O \quad (7)$$

In conclusion, this catalytic reaction could be predominantly performed using the E–R mechanism and the L–H mechanism.

3. Materials and Methods

3.1. Catalyst Preparation

The pH-modified catalysts were prepared as follows. Ammonium hydroxide (25–28%) (AR, 99.5%, Tianjin Fuchen Chemicals Co., Ltd., Tianjin, China) was used to adjust the pH between 2.5 and 11 under continuous stirring for 30 min. The original pH of the synthesis mixture was 2.5, which was also considered for comparison. Finally, the container was put in an oven at 110 °C for 4–5 h and calcined in air at 500 °C for 3 h. The original V_2O_5-MoO_3/TiO_2 catalyst is prepared using the wet impregnation method. NH_4VO_3 (AR, 99.0%, Tianjin Fuchen Chemicals Co., Ltd., China) was added to an oxalic acid ($H_2C_2O_4$, AR, 99.5%, Tianjin Fuchen Chemicals Co., Ltd., China) solution under stirring until the color of the solution changed gradually from orange to dark blue. The mole ratio of NH_4VO_3 and $H_2C_2O_4$ was 1:2. $(NH_4)_2MoO_4$ (AR, 99.5%, Tianjin Fuchen Chemical Co., Ltd., China) was then added, followed by TiO_2 (98%, Sinopharm Chemical Reagent Co., Ltd., Shanghai, China), and the obtained catalyst slurry was then continued to stir for 2 h. Finally, the catalyst slurry was placed into an oven, dried at 110 °C for 4–5 h, and calcined under air at 500 °C for 3 h. The mass fraction of V_2O_5 and MoO_3 was 3 and 6 wt%, respectively. After cooling, the catalysts were sieved with a 20–40 mesh sieve and prepared for the test.

The Co-modified catalysts were also prepared using the impregnation method. The primary distinction between the cobalt-modified catalyst and the VMT catalyst lies in the former's introduction of a requisite mass percentage of $(CH_3COO)_2Co$ (AR, 99.5%, Tianjin Fuchen Chemicals Co., Ltd., China) subsequent to the addition of $(NH_4)_2MoO_4$, but prior to the inclusion of TiO_2.

For the pH-modified catalysts prepared in this paper, after preparing the catalyst precursor solution the pH of the resulting solution was adjusted with ammonium hydroxide (NH_4OH, 25–28%, AR, Tianjin Fuchen Chemicals Co., Ltd., Tianjin, China). The level selected for the pH was between 9 and 11. The original pH of the synthesis mixture was 2.5. The drying and calcination of the modified catalyst slurries were conducted in the same manner as the treatment of the original catalyst. In addition, to ensure experimental reproducibility, the modified catalysts were dried and calcined under the same conditions as the original catalyst (dried at 110 °C for 4–5 h and calcined in air at 500 °C for 3 h).

3.2. Catalytic Activity

NO conversion was carried out in a fixed-bed glass reactor (φ = 20 mm), and the required reaction temperature was controlled using an electric furnace. The amount of catalyst in each test was 2 g, and the total amount of flue gas was 1.50 L/min, with a gas hourly space velocity of 30,000 h^{-1}. The reaction gas composition was 0.07 vol% NO_x, 0.07 vol% NH_3, and 5 vol% O_2, while N_2 was used as the carrier gas. The following reaction in the flue gas occured:

$$4NO + 4NH_3 \rightarrow O_2 + 4N_2 + 6H_2O \quad (8)$$

A nitrogen oxide analyzer (High Level 42i, Thermal Electron Co., Waltham, MA, USA) was used to test the concentration of NO_x and calculate its conversion rate. A pH tester (WTW Multi3620, Burladingen, Germany) was used to control the pH of the catalyst slurry. The conversion of NO_x was calculated as follows:

$$NO_x \text{ conversion } \% = \frac{[NO_x]_{in} - [NO_x]_{out}}{[NO_x]_{in}} \times 100\% \text{ (Assume } Q_1 = Q_2) \quad (9)$$

where $[NO_x]_{in}$ and $[NO_x]_{out}$ represent the concentrations of NO_x of the inlet and outlet gas streams, respectively, while Q_1 and Q_2 represent the flow rates of the inlet and outlet, respectively.

3.3. Structure Characterizations

The Brunauer–Emmett–Teller (BET) and Barret–Joyner–Halenda (BJH) methods were used to measure the specific surface area by N_2 adsorption with a Micromeritics Gemini V instrument (Norcross, GA, USA). After preparation, the samples were degassed under a vacuum at 110 °C for 1 h.

X-ray diffraction (XRD) patterns were obtained with a Bruker D8 Advance instrument (Billerica, MA, USA) employing a Ni-filtered Cu *Kα* (λ = 0.15406) radiation. The spectra were registered between 10 and 90° with a step of 0.02°.

X-ray photoelectron spectroscopy (XPS) measurements were carried out on a Thermo–Fisher Scientific K-Alpha+ instrument (Waltham, MA, USA) under an ultravacuum at a pressure lower than 5×10^{-6} Pa. A monochromatic Al Kα X-ray source (1486.6 eV) at a power of 15 kV (15 mA) was used for the analysis.

Temperature-programmed reduction with hydrogen (H_2-TPR) was carried out using a Micrometritics Auto-Chem II 2920 instrument (Norcross, GA, USA). For the measurements, a 10% H_2 and 90% Ar mixture was used, the heating rate was 10 °C/min, and the samples were pretreated at 300 °C. The consumption of H_2 was detected with a thermal conductivity detector.

Temperature-programmed desorption with ammonia (NH_3-TPD) was carried out with a Chem-BET Pulsar TPR/TPD instrument (Quantachrome, Boynton Beach, FL, USA). After pretreatment at 300 °C for 1 h, the samples were saturated with pure NH_3 vapor at ambient temperature, then purged with He as the temperature was increased at a rate of 10 °C/min.

In situ diffuse reflectance infrared Fourier-transform spectroscopy (In situ DRIFTS) data were collected by accumulating 64 scans at a resolution of 4 cm^{-1}. The spectra were acquired using an in situ DRIFTS cell equipped with a gas flow system (Bruker Tensor II, Billerica, MA, USA). The samples were pretreated at 300 °C under N_2 for 1 h and then cooled to room temperature.

4. Conclusions

Modified catalysts with pH regulation and Co doping can be synthesized using the wet impregnation method. The 1CoVMT-10 catalyst exhibited optimal denitrification activity when the pH was 10 and the molar fraction of Co doping was 1 wt%.

The pH regulation method could improve the dispersion of the particles and the uniformity on TiO_2. Both pH regulation and cobalt doping methods can convert polymeric vana-

dium to an isolated form, and the increased V^{5+}=O species resulted in more Brønsted and Lewis acid sites for NH_3 and NO_x adsorbed species on the surface of the catalyst, promoting SCR activity. The ratios of Co^{2+}/Co^{3+} and V^{5+}/V^{4+} developed, and abundant V^{5+} and Co^{2+} were beneficial for facilitating the SCR reaction cycle in the $Co^{2+} + V^{5+} \rightarrow Co^{3+} + V^{4+}$ process. In addition, both O_β and O_α could promote the participation of active substances in the process of oxidizing NO to NO_2, theoretically making the rapid SCR cycling reaction easier to occur in terms of VMT-10 and 1CoVMT-10, respectively. Combined with the NH_3-TPD and DRIFTS studies, the results suggest that the NH_3 and NO_2 adsorbed species on the surface of 1CoVMT-10 have higher activity in the SCR reaction than VMT. The developed amount of medium and strong Lewis acidic sites showed an intensive effect in terms of NH_3 adsorption. Furthermore, the DRIFTS study indicated that the NH_3-SCR reaction over 1CoVMT-10 followed the E–R and L–H mechanism.

Supplementary Materials: The following supporting information can be downloaded at: https://www.mdpi.com/article/10.3390/catal13050844/s1, Figure S1: BET fitting curve of VMT catalyst; Figure S2: H_2-TPR profiles of the catalyst samples: (a) VMT; (b) VMT-10; (c) 1CoVMT-10; Table S1: NO removal efficiency under laboratory conditions of Co-doped or pH-regulated catalysts; Table S2: Peak area of vanadyl species species from fitting data.

Author Contributions: Conceptualization, R.W. and Y.Z.; methodology, R.W.; software, R.W. and Y.Z.; validation, R.W.; formal analysis, R.W.; investigation, R.W.; resources, R.W. and Y.Z.; data curation, R.W.; writing—original draft preparation, R.W.; writing—review and editing, J.L.; visualization, X.F.; supervision, X.F. and J.L.; project administration, J.L.; funding acquisition, J.L. All authors have read and agreed to the published version of the manuscript.

Funding: This research was funded by the National Key Research and Development Program of China (No.2017YFC0210303).

Data Availability Statement: The data presented in this study are available in article and Supplementary Material.

Conflicts of Interest: The authors declare no conflict of interest.

References

1. Wu, Y.X.; Liang, H.L.; Chen, X.; Chen, C.; Wang, X.Z.; Dai, C.Y.; Hu, L.M.; Chen, Y.F. Effect of preparation methods on denitration performance of V-Mo/TiO_2 catalyst. *J. Fuel Chem. Technol.* **2020**, *48*, 189–196. [CrossRef]
2. Zheng, Y.J.; Jensen, A.D.; Johnsson, J.E. Deactivation of V_2O_5-WO_3-TiO_2 SCR catalyst at a biomass-fired combined heat and power plant. *Appl. Catal. B-Environ.* **2005**, *60*, 253–264. [CrossRef]
3. Nova, I.; Dall Acqua, L.; Lietti, L.; Giamello, E.; Forzatti, P. Study of thermal deactivation of a de-NO_x commercial catalyst. *Appl. Catal. B-Environ.* **2001**, *35*, 31–42. [CrossRef]
4. Zhang, S.; Li, H.Y.; Zhong, Q. Promotional effect of F-doped V_2O_5-WO_3/TiO_2 catalyst for NH_3-SCR of NO at low-temperature. *Appl. Catal. A.-Gen.* **2012**, *435–436*, 156–162. [CrossRef]
5. Zhao, W.; Zhong, Q.; Pan, Y.X.; Zhang, R. Systematic effects of S-doping on the activity of V_2O_5/TiO_2 catalyst for low-temperature NH_3-SCR. *Chem. Eng. J.* **2013**, *228*, 815–823. [CrossRef]
6. Gao, Y.; Wu, X.D.; Ran, R.; Si, Z.C.; Ma, Z.R.; Wang, B.D.O.; Weng, D. Effects of MoO_x on dispersion of vanadia and low-temperature NH_3-SCR activity of titania supported catalysts: Liquid acidity and steric hindrance. *Appl. Surf. Sci.* **2022**, *585*, 152710. [CrossRef]
7. Jae, G.H.; Mahboob, U.; Chun, M.; Yong, S.C.; Seong, G.S.; Min, C.S.; Young, S.C.; Kim, D. Low-temperature shift $DeNO_x$ activity of Nanoflake V_2O_5 loaded WO_3/TiO_2 as NH_3-SCR catalyst. *Inorg. Chem. Commun.* **2022**, *137*, 109191. [CrossRef]
8. Liu, F.; He, H.; Lian, Z.; Shan, W.; Xie, L.; Asakura, K.; Yang, W.; Deng, H. Highly dispersed iron vanadate catalyst supported on TiO_2 for the selective catalytic reduction of NO_x with NH_3. *J. Catal.* **2013**, *307*, 340–351. [CrossRef]
9. Lónyi, F.; Solt, H.E.; Valyon, J.; Boix, A.; Gutierrez, L.B. The SCR of NO with methane over In,H- and Co,In,H-ZSM-5 catalysts: The promotional effect of cobalt. *Appl. Catal. B-Environ.* **2012**, *117–118*, 212–223. [CrossRef]
10. Kubacka, A.; Janas, J.; Sulikowski, B. In/Co-ferrierite: A highly active catalyst for the CH_4-SCR NO process under presence of steam. *Appl. Catal. B-Environ.* **2006**, *69*, 43–48. [CrossRef]
11. Xue, H.Y.; Guo, X.M.; Meng, T.; Mao, D.S.; Ma, Z. NH_3-SCR of NO over M/ZSM-5 (M = Mn, Co, Cu) catalysts: An in-situ DRIFTS study. *Surf. Interfaces* **2022**, *29*, 101722. [CrossRef]
12. Kimihiro, A.; Chie, O.; Shinji, I.; Yasushi, S.; Masashi, I. Potassium-doped Co_3O_4 catalyst for direct decomposition of N_2O. *Appl. Catal. B-Environ.* **2008**, *78*, 242–249. [CrossRef]

13. Bo, Z.; Zhu, J.; Yang, S.; Yang, H.; Yan, J.; Cen, K. Enhanced plasma-catalytic decomposition of toluene over Co-Ce binary metal oxide catalysts with high energy efficiency. *RSC Adv.* **2019**, *9*, 7447–7456. [CrossRef] [PubMed]
14. Zhao, H.; Han, W.; Tang, Z. Tailored design of high-stability $CoMn_{1.5}O_x$@TiO_2 double-wall nanocages derived from Prussian blue analogue for catalytic combustion of o-dichlorobenzene. *Appl. Catal. B-Environ.* **2020**, *276*, 119133. [CrossRef]
15. Zhao, H.W.; Yang, G.P.; Hill, A.J.; Luo, B.E.; Jing, G.H. One-step ion-exchange from Na-SSZ-13 to Cu-SSZ-13 for NH_3-SCR by adjusting the pH value of Cu-exchange solution: The effect of H^+ ions on activity and hydrothermal stability. *Microporous Mesoporous Mat.* **2021**, *324*, 111271. [CrossRef]
16. Fan, A.; Jing, Y.; Guo, J.; Shi, X.; Yuan, S.; Li, J. Investigation of Mn doped perovskite La-Mn oxides for NH_3-SCR activity and SO_2/H_2O resistance. *Fuel* **2022**, *310*, 122237. [CrossRef]
17. Besselmann, S.; Löffler, E.; Muhler, M. On the role of monomeric vanadyl species in toluene adsorption and oxidation on V_2O_5/TiO_2 catalysts: A Raman and in situ DRIFTS study. *Mol. Catal.* **2000**, *162*, 401–411. [CrossRef]
18. Qiu, Y.; Liu, B.; Du, J.; Tang, Q.; Liu, Z.H.; Liu, R.L.; Tao, C.Y. The monolithic cordierite supported V_2O_5-MoO_3/TiO_2 catalyst for NH_3-SCR. *Chem. Eng. J.* **2016**, *294*, 264–272. [CrossRef]
19. Pulido Melián, E.; González Díaz, O.; Ortega Méndez, A.; López, C.R.; Nereida Suárez, M.; Doña Rodríguez, J.M.; Navío, J.A.; Fernández Hevia, D.; Pérez Peña, J. Efficient and affordable hydrogen production by water photo-splitting using TiO_2-based photocatalysts. *Int. J. Hydrogen Energy* **2013**, *38*, 2144–2155. [CrossRef]
20. Bulushev, D.A.; Kiwi-Minsker, L.; Rainone, F.; Renken, A. Characterization of surface vanadia forms on V/Ti-oxide catalyst via temperature-programmed reduction in hydrogen and spectroscopic methods. *J. Catal.* **2002**, *205*, 115–122. [CrossRef]
21. Tang, F.S.; Zhuang, K.; Yang, F.; Yang, L.L.; Xu, B.L.; Qiu, J.H.; Fan, Y.N. Effect of dispersion state and surface properties of supported vanadia on the activity of V_2O_5/TiO_2 catalysts for the selective catalytic reduction of NO by NH_3. *Chin. J. Catal.* **2012**, *33*, 933–940. [CrossRef]
22. Topsoe, N.Y.; Topsoe, H.; Dumesic, J.A. Vanadia/titania catalysts for selective catalytic reduction (SCR) of nitric-oxide by ammonia: I. combined temperature-programmed in-situ FTIR and on-line mass-spectroscopy studies. *J. Catal.* **1995**, *151*, 226–240. [CrossRef]
23. Yu, C.; Huang, B.; Dong, L.; Chen, F.; Yang, Y.; Fan, Y.; Yang, Y.; Liu, X.; Wang, X. Effect of Pr/Ce addition on the catalytic performance and SO_2 resistance of highly dispersed MnO_x/SAPO-34 catalyst for NH_3-SCR at low temperature. *Chem. Eng. J.* **2017**, *316*, 1059–1068. [CrossRef]
24. Li, X.; Niu, Y.; Li, J.; Yang, M.; Chen, R.; Shao, D.; Zheng, X.; Zhang, C.; Qi, Y. Trace Co doping improves NH_3-SCR performance and poisoning resistance of Ce-Mn-based catalysts. *Chem. Eng. J.* **2023**, *454*, 140180. [CrossRef]
25. Chen, Q.; Guo, R.; Wang, Q.; Pan, W.; Yang, N.; Lu, C.; Wang, S. The promotion effect of Co doping on the K resistance of Mn/TiO_2 catalyst for NH_3-SCR of NO. *J. Taiwan Inst. Chem. Eng.* **2016**, *64*, 116–123. [CrossRef]
26. Wu, R.; Li, L.; Zhang, N.; He, J.; Song, L.; Zhang, G.; Zhang, Z.; He, H. Enhancement of low-temperature NH_3-SCR catalytic activity and H_2O & SO_2 resistance over commercial V_2O_5-MoO_3/TiO_2 catalyst by high shear-induced doping of expanded graphite. *Catal. Today* **2021**, *376*, 302–310. [CrossRef]
27. Chen, Y.; Chen, Z.; Zhang, C.; Chen, L.; Tang, J.; Liao, Y.; Ma, X. Multiple pollutants control of NO, benzene and toluene from coal-fired plant by Mo/Ni impregnated TiO_2-based NH_3-SCR catalyst: A DFT supported experimental study. *Appl. Surf. Sci.* **2022**, *599*, 153986. [CrossRef]
28. Gao, F.; Tang, X.; Yi, H.; Li, J.; Zhao, S.; Wang, J.; Chu, C.; Li, C. Promotional mechanisms of activity and SO_2 tolerance of Co-or Ni-doped MnO_x-CeO_2 catalysts for SCR of NO_x with NH_3 at low temperature. *Chem. Eng. J.* **2017**, *317*, 20–31. [CrossRef]
29. Chen, M.; Zheng, X. Effect of promoter thallium for a novel selectivity oxidation catalyst studied by X-ray photoelectron spectroscopy. *J. Mol. Catal.* **2003**, *201*, 161–166. [CrossRef]
30. Xi, X.Y.; Zeng, F.; Zhang, H.; Wu, X.F.; Ren, J.; Bisswanger, T.; Stampfer, C.; Hofmann, J.P.; Palkovits, R.; Heeres, H.J. CO_2 hydrogenation to higher alcohols over K-promoted bimetallic Fe-In catalysts on a Ce-ZrO_2 support. *ACS Sustain. Chem. Eng.* **2021**, *9*, 6235–6249. [CrossRef]
31. Qiu, L.; Pang, D.D.; Zhang, C.L.; Meng, J.J.; Zhu, R.S.; Ouyang, F. In situ IR studies of Co and Ce doped Mn/TiO_2 catalyst for low-temperature selective catalytic reduction of NO with NH_3. *Appl. Surf. Sci.* **2015**, *357*, 189–196. [CrossRef]
32. Kang, S.H.; Ryu, J.H.; Kim, J.H.; Sai Prasad, P.S.; Bae, J.W.; Cheon, J.Y.; Jun, K.W. ZSM-5 supported cobalt catalyst for the direct production of gasoline range hydrocarbons by Fischer-Tropsch synthesis. *Catal. Lett.* **2011**, *141*, 1464–1471. [CrossRef]
33. Lonyi, F.; Valyon, J. On the interpretation of the NH_3-TPD patterns of H-ZSM-5 and H-mordenite. *Microporous Mesoporous Mat.* **2001**, *47*, 293–301. [CrossRef]
34. Dong, G.; Zhang, Y.F.; Zhao, Y.; Bai, Y. Effect of the pH value of precursor solution on the catalytic performance of V_2O_5-WO_3/TiO_2 in the low temperature NH_3-SCR of NO_x. *J. Fuel Chem. Technol.* **2014**, *42*, 1455–1463. [CrossRef]
35. Centeno, M.A.; Carrizosa, I.; Odriozola, J.A. In situ DRIFTS study of the SCR reaction of NO with ammonia over a high loading (15% weight) vanadia-titania catalyst. *Phys. Chem. Chem. Phys.* **1999**, *1*, 349–354. [CrossRef]
36. Chen, Z.D.; Li, N.; Zhang, K.; Hou, L.M.; Wu, W.F. In-situ infrared spectroscopic study of the mechanism of the low temperature selective catalytic reduction of NO surface by Mn/bastnaesite concentrate. *Int. J. Hydrogen Energy* **2022**, *47*, 24777–24795. [CrossRef]
37. Wang, J.P.; Yan, Z.; Liu, L.L.; Chen, Y.; Zhang, Z.T.; Wang, X.D. In situ DRIFTS investigation on the SCR of NO with NH_3 over V_2O_5 catalyst supported by activated semi-coke. *Appl. Surf. Sci.* **2014**, *313*, 660–669. [CrossRef]

38. Dall'Acqua, L.; Nova, I.; Lietti, L.; Ramis, G.; Busca, G.; Giamello, E. Spectroscopic characterisation of MoO_3/TiO_2 denox-scr catalysts: Redox and coordination properties. *Phys. Chem. Chem. Phys.* **2000**, *2*, 4991–4998. [CrossRef]
39. Sun, D.; Liu, Q.; Liu, Z.; Gui, G.; Huang, Z. An In Situ DRIFTS Study on SCR of NO with NH_3 Over V_2O_5/AC Surface. *Catal. Lett.* **2009**, *132*, 122–126. [CrossRef]
40. Primet, M.; Pichat, P.; Mathieu, M.V. Infrared study of the surface of titanium dioxides. I. Hydroxyl groups. *J. Phys. Chem.* **1971**, *75*, 1216–1220. [CrossRef]
41. Liu, K.; Liu, F.; Xie, L.; Shan, W.; He, H. DRIFTS study of a Ce-W mixed oxide catalyst for the selective catalytic reduction of NO_x with NH_3. *Catal. Sci. Technol.* **2015**, *5*, 2290–2299. [CrossRef]
42. Karami, A.; Salehi, V. The influence of chromium substitution on an iron-titanium catalyst used in the selective catalytic reduction of NO. *J. Catal.* **2012**, *292*, 32–43. [CrossRef]
43. Chen, L.; Li, J.; Ge, M. DRIFT Study on Cerium-Tungsten/Titiania Catalyst for Selective Catalytic Reduction of NO_x with NH_3. *Environ. Sci. Technol.* **2010**, *44*, 9590–9596. [CrossRef] [PubMed]
44. Chen, H.Y.; Voskoboinikov, T.; Sachtler, W.M.H. Reduction of NO_x over Fe/ZSM-5 catalysts: Mechanistic causes of activity differences between alkanes. *Catal. Today* **1999**, *54*, 483–494. [CrossRef]
45. Frost, R.L. An infrared and Raman spectroscopic study of the uranyl micas. *Spectroc. Acta Part A-Molec. Biomolec. Spectr.* **2004**, *60*, 1469–1480. [CrossRef] [PubMed]
46. Li, Y.J.; Slager, T.L.; Armor, J.N. Selective reduction of NO_x by methane on Co-Ferrierites: II. catalyst characterization. *J. Catal.* **1994**, *150*, 388–399. [CrossRef]
47. Aylor, A.W.; Lobree, L.J.; Reimer, J.A.; Bell, A.T. An infrared study of NO reduction by CH_4 over Co-ZSM-5. *Stud. Surf. Sci. Catal.* **1996**, *101*, 661–670. [CrossRef]
48. Amblard, M.; Burch, R.; Southward, B.W.L. A study of the mechanism of selective conversion of ammonia to nitrogen on $Ni/\gamma\text{-}Al_2O_3$ under strongly oxidising conditions. *Catal. Today* **2000**, *59*, 365–371. [CrossRef]
49. Zhu, Z.P.; Liu, Z.Y.; Niu, H.X.; Liu, S.J. Promoting effect of SO_2 on activated carbon-supported vanadia catalyst for NO reduction by NH_3 at low temperatures. *J. Catal.* **1999**, *187*, 245–248. [CrossRef]
50. Abello, L.; Husson, E.; Repelin, Y.; Lucazeau, G. Vibrational spectra and valence force field of crystalline V_2O_5. *Spectroc. Acta Part A-Molec. Biomolec. Spectr.* **1983**, *39*, 641–651. [CrossRef]
51. Topsøe, N.; Topsøe, H. Combined in-situ FTIR and on-line activity studies: Applications to vanadia-titania $DeNO_x$ catalyst. *Catal. Today* **1991**, *9*, 77–82. [CrossRef]